An Infrared Stellar Thermometer

Ieva Puspure

Lund Observatory
Lund University

2021-EXA178

Degree project of 15 higher education credits
June 2021

Supervisors: Nils Ryde and Brian Thorsbro

Lund Observatory
Box 43
SE-221 00 Lund
Sweden

Abstract

Infrared (IR) spectroscopy has many advantages over optical, one of which is allowing us to see through intergalactic dust, letting us probe deeper into space and dust-dense regions such as galactic centers. However the investigating the IR spectral range is a relatively new field, owing to recent developments in detector technology, and stellar parameter determination in IR is not well researched. This thesis aims to explore stellar temperature determination in this spectral range.

Temperature can be considered as one of the most important stellar parameters, as it is crucial to know when determining chemical abundances, and it allows us to classify stars from which we may then analyse individual bodies and stellar populations. A variety of methods exist for determination, however in this thesis we use spectral synthesis.

We determine the effective temperature through spectral synthesis done with high resolution and high signal-to-noise ratio H-band (1.5–1.8 microns) spectra taken by the IGRINS spectrometer of 12 K-giants, with a range of temperatures between 4100–5200 K and metallicites between -0.80–0.30 dex. We use stellar parameters from Jönnson et. al. (in prep) determined in the optical range for modelling stellar atmospheres, and as a benchmark for stellar temperatures.

We find that only using Fe I absorption lines for spectral synthesis produces poor results in comparison, and choose to additionally look at CO molecular lines, using carbon and oxygen abundances found in Jönnson et. al. (in prep.). While these produce temperatures closer to the benchmark, the best results are found from a combination of Fe I and CO lines which give temperatures on average 40 K higher with $\sigma = 24$ K.

Acknowledgements

I would like to extend my upmost gratitude to my supervisor Nils Ryde, and co-supervisor Brian Thorsbro for their guidance. This thesis would not have been possible without their counsel and their humor that frequently lifted my spirits in this difficult time. I would also like to thank other members of the ISA group: Martin Montelius, Henrik Jönnson and Rebecca Forsberg for their additional support.

Popular science summary

Millions of stars litter the night sky, and our understanding of how they were born is still developing. These burning orbs of gas are so far away that even the light they give off takes years to arrive to us on Earth. So how are we to measure anything about them if sending any equipment to their distant locations is unimaginable? Since the days of Newton, the only way we have been able to say anything about stars has been by looking at the colour of their light.

While stars appear to glow in a single colour to us, they are a mixture of many colours. By dispersing the light of stars, we can see that certain colours that make up the light are not as bright as others; each of the elements that make up a star will absorb certain colours of light more than other colours. How much light is absorbed will depend on how hot the star is, and by finding patterns in the light absorption we can determine the exact temperature, creating somewhat of a long-distance thermometer.

Equipment both in space and on Earth, such as the famous Hubble Telescope, measure how brightly stars glow through different colour filters. We have researched this extensively in visible light, however the light stars emit goes beyond what we can see with our naked eye, such as infrared.

We have developed computer programs that can find out star temperatures from light measurements, but we are not exactly sure which element patterns are best to look at in infrared for finding temperature; studying this will allow us to use upcoming instruments, such as the James Webb Space Telescope, to their full potential.

By understanding how best to utilise infrared measurements, we also increase how much of space we can see, as light visible to the naked eye can often be blocked by clouds of dust that litter space. This is not as large of a problem for infrared light, as it can travel through dust much better than visible light. Because of this we can use thermal cameras to see people through smoke for example, as anything with heat will also release infrared light. Deepening our understanding of the infrared range will allow us to broaden our horizons in our understanding of even the most distant stars.

Contents

List of Figures

List of Tables

Chapter 1

Introduction

Spectroscopy has been an important part of astronomy since Newton showed sunlight refracted through a prism in 1670. By dispersing light into a spectrum, we are able to look at the wavelengths of light the source emits. It was based on this mechanism that spectroscopy was birthed in 1800s, when dark lines were seen in the Sun's spectrum by Josef von Fraunhofer (Fraunhofer 1815). The lines were later found to be atomic absorption lines; electrons in atoms absorb photons of wavelengths corresponding to the energy required to move to a higher energy level. This causes the light in that specific wavelength to be dimmer than in the rest of the spectrum. These energy levels (and thus photon wavelengths of absorption lines) are specific to atom species (Harrison 2011).

Stellar spectroscopy has only advanced since, and with improvements in detector technology has expanded beyond the classical optical range, of which the Sun's spectrum can be seen in Figure 1.1. Other major wavelength bands have included radio and x-ray ranges, allowing us to look at space from many different perspectives. Each spectral band is a field of study of its own, with different technology and analytical methods involved. A more recent development in spectroscopy is concerned with the infrared (IR) range of the electromagnetic spectrum, ranging from near infrared (NIR) to mid infrared (approximately 1 micron to beyond 10 microns).

By looking at stellar spectra we can see spectral lines formed in the star's atmosphere: light formed in the deeper layers of the star is a spectrum, shaped approximately like that of a black body radiator of the same temperature. This passes through the atmosphere, where various atoms will absorb certain wavelengths corresponding to their energy level transitions. Looking at the profiles of absorption lines in a stellar spectrum, we can characterise the star's atmosphere and determine parameters such as gravity, the effective temperature of the star, and chemical abundances, as these affect the shape of spectral lines in different ways. Arguably one of the most important of these parameters is the effective temperature; for absorption lines typically used in chemical abundance determination, temperature plays a large role in the shape of the line, and beyond that, with temperature we can classify stars to look at the evolution of individual bodies as well as stellar populations (Matteucci 2001).

The aim of this thesis is to explore how well we can determine effective temperature

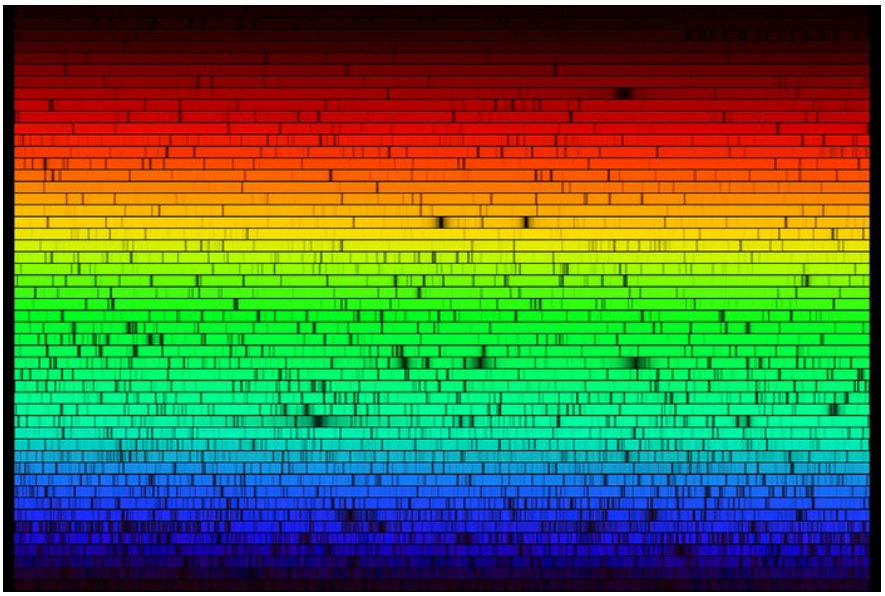

Figure 1.1: Visible wavelength spectrum of the Sun. Each dark line is caused by absorption of photons in atomic transitions. Source: NOAO/AURA/NSF

of a certain class of red giants by using stellar spectra in the H-band (1.5 to 1.8 microns). Temperature affects the number of atoms at given excitation levels (known as level populations) and thus the spectral lines we see. The temperature determination will be done by creating synthetic spectra and comparing them to observed spectra until the strength of spectral lines in the given range match, utilising the fact that iron lines as well as lines from molecules such as CO are abundant in this wavelength region and particularly temperature sensitive (see e.g. Schultheis et al. (2016)). Iron abundance will be simultaneously determined as it is linked to the temperature in the method used in this thesis.

1.1 Infrared Spectroscopy

One of the problems in traditional visible-range spectroscopy is that of interstellar dust which sits between us, and many far away regions of space. Dust can do various things to light passing through it; it can absorb light or scatter it. The effects vary depending on the wavelength of the light passing through the dust, and amount of dust travelled through. Light of shorter wavelengths gets scattered and absorbed more than longer wavelengths, in effect reddening the light.

This effect hinders optical observations of stellar populations obscured by dust. Such is the case for distant stars with dust on the path of observation, or particularly dust dense regions like the centers of galaxies. Astronomers can circumvent this problem by looking at infrared light which does not get scattered or absorbed as much, penetrating the previously stated obstacle. While infrared astronomy is not new, infrared spectroscopy specifically is only a recent development and is thus not well studied (Rieke 2009).

There are other advantages to looking at stars through IR-wavelengths. Red giants are some of the brightest stars in the infrared range allowing their light to travel further than that of smaller stars. IR-lights' dust penetrating properties also make red giants the perfect probes when looking at dust-dense star forming regions for example. With red giants, we can see both further out in space, and into regions we may not observe otherwise through traditional visible range spectroscopy.

An extra advantage of looking at red giants is that as stars become cooler (with temperatures lower than 6000 K), molecules form and their absorption lines can be seen in stellar spectra (Masseron 2015).K-type giants especially are cool enough to contain temperature sensitive molecules such as CO (Schultheis et al. 2016). However, a problem arises for the even cooler M-type giants, as in that case the the spectral lines from molecules may crowd the spectrum, making analysis more difficult (Jönsson et al. 2017).

The delay in the advancement of IR spectroscopy can be accounted for by the available technology; the most widely used detectors are silicon based charged couple devices (CCDs) which detect in the range of 0.2 to 1.1 microns (Horiba 2021). The detector is transparent to any longer wavelengths as the bandgap of the detector becomes greater than the photon energy. Recent development of detector materials such as mercury cadmium telluride (HgCdTe), initially used in military applications of thermal imaging, have allowed us to probe this previously unexplored region of wavelengths (Longshore 2002).

Recent and upcoming telescopes, such as the Stratospheric Observatory for Infrared Astronomy (SOFIA), and the James Webb Space Telescope (JWST) as well as ground-based telescopes are equipped with such detectors (Rieke 2009). As such, it is important to explore stellar parameter methods in these wavelengths so that the measurements taken in these surveys may be used to their full potential.

1.2 Stellar parameters

There are several parameters that characterize a star, however these are difficult to define; stars are not uniform in temperature, and their size is defined by the region light can escape from. The light we see from stars originates from its atmosphere. This region is defined as the transition between the stellar interior and interstellar medium. Stellar atmospheres can be divided into several parts, and the spectra we see from stars originates from the region known as the photosphere. The photosphere is hot deep within the star, and progressively gets cooler as we travel outwards, however a significant temperature rise can be seen in the regions that follow; the chromosphere and the corona. The photosphere is the first optically thin enough region to allow light to escape. This defines somewhat of a "visual" surface, as the actual depth at which light escapes depends on several parameters, such as the wavelength of the light (Gray 2008).

We can replace this "visual" radius measurement with that in terms of a star's mass and surface gravity:

$$g = G\frac{M}{R^2} \tag{1.1}$$

where G is the gravitational constant, and M and R are the mass and radius of the star respectively.

1.2.1 Effective temperature

As described previously, stars do not have a uniform temperature, however it is possible to define a unique temperature tied to the power output, called effective temperature T_{eff}. It is defined in terms of the total power output of the star per unit area, (Gray 2008):

$$\int_0^\infty \mathfrak{F}_\nu \, \mathrm{d}\nu = \sigma T_{\text{eff}}^4 \tag{1.2}$$

where the flux exiting the star $\mathfrak{F}$ integrated over all light frequencies ν (defined as bolometric flux) gives the effective temperature T_{eff} multiplied by the Stefan-Boltzmann constant σ. This formula has the same form as the Stefan-Boltzmann law; if a black-body radiator were to have the same total flux output, it would have the same temperature as the star. We can further relate the temperature to the luminosity (L) of a star using its radius R (Gray 2008):

$$L = 4\pi R^2 \int_0^\infty \mathfrak{F}_\nu \, \mathrm{d}\nu = 4\pi R^2 \sigma T_{\text{eff}}^4 \tag{1.3}$$

The radius of the star may be determined through interferometry, comparing the luminosity to that of the Sun, or through other methods. The effective temperature is fundamentally determined by the mass, evolutionary stage, and composition of the star.

The relative strengths and shapes of spectral lines vary with temperature. For example, hydrogen Balmer lines (transitions from the second energy and up of neutral hydrogen) get stronger with increasing stellar temperatures, with a maximum strength between 7500 – 10000 K, after which they decrease in strength. Below these temperatures, not much hydrogen is in the second energy level, and at higher temperatures, hydrogen is mostly ionized; due to this we find a maximum line strength at a certain temperature.

From this we can derive a classification system of stars according to temperature from hottest to coolest in the following classical sequence: O, B, A, F, G, K, M, with further numerical subdivisions for each letter (Gray 2008). This system has been extended even further in modern times.

By plotting the luminosity of a star (or absolute magnitude, the brightness at a distance of 10 pc to us) against its temperature, we can classify stars by size in addition to temperature. This is referred to as a Hertzsprung-Russel diagram (HR-diagram), an example can be seen in Figure 1.2. Stars appear in various regions of the diagram depending on their size and spectral type giving us further subcategories such as main sequence stars or giants.

1.2.2 Metallicity

In astronomy, any elements heavier than hydrogen and helium are considered metals. Metallicity thus describes the ratio of metal atoms to H and He atoms. If a similar chemical

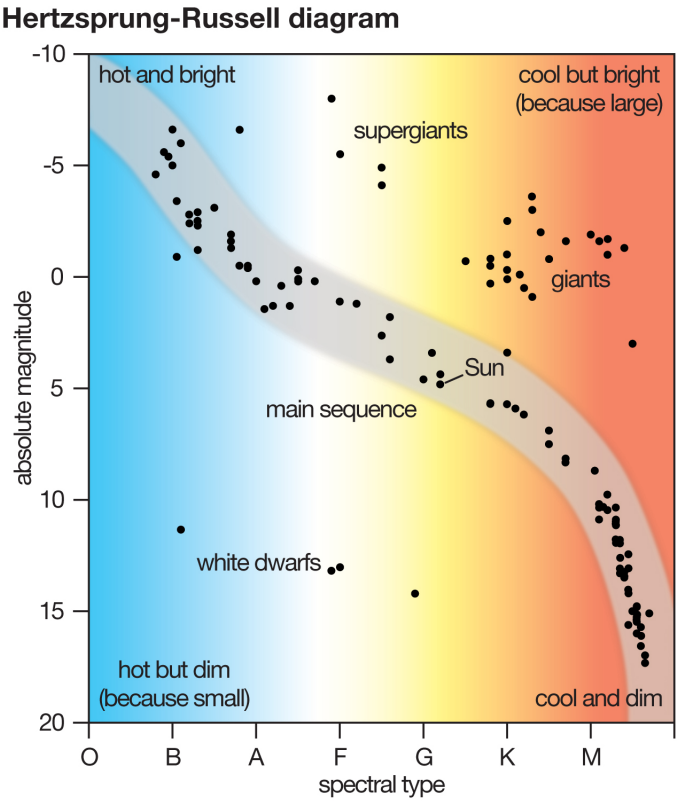

Figure 1.2: Reference Hertzsprung-Russel diagram plotting the absolute magnitude against the spectral type of different stars. The stars can be classified according to what region they are on the diagram, with magnitude (dependent on luminosity) determining the size according to equation (1.3). Source: Encyclopædia Britannica (2021)

distribution to the Sun is assumed, we can use iron abundance as a proxy to metallicity. This is typically done as iron lines are some of the most prevalent in stellar spectra. The iron abundance (and thus metallicity) of a star can be described in comparison to that of the Sun as below (see e.g. Matteucci (2001)):

$$[\mathrm{Fe/H}] = \log\left(N_{\mathrm{Fe}}/N_{\mathrm{H}}\right)_{\mathrm{Star}} - \log\left(N_{\mathrm{Fe}}/N_{\mathrm{H}}\right)_{\mathrm{Sun}} \tag{1.4}$$

where N is the number of atoms per unit of volume for their respective elements. Metallicity is given in units of "dex", stars with a metallicity of -1.0 dex are 10 times less metal abundant than the Sun.

1.3 Spectral line formation

To extract information about a star from its spectrum, we must understand what affects spectral line formation. The following sections discuss what role temperature plays in this.

1.3.1 Level populations

We must first acknowledge the quantum processes behind spectral line formation. The most relevant in spectroscopy is understanding the statistics behind atomic level populations and the ratios of neutral to ionized atoms, as both will affect the strength of spectral lines. We assume that in the photosphere collisions dominate the mechanism of level population (as opposed to non-thermal radiative excitation), and describe the relative level populations as below:

$$\frac{N_n}{N_m} = \frac{g_n}{g_m} \mathrm{e}^{-\Delta\chi/kT} \tag{1.5}$$

where n and m are two different excitation levels in an atom; $g = 2J + 1$ is the statistical weight of each level where J is the J quantum number; $\Delta\chi = \chi_n - \chi_m$ is the difference in excitation potential; k is the Boltzmann constant; and T is the temperature. This defines a clear relation between level populations and temperature (Gray 2008).

In regards to ionization levels, we use the Saha function which relates the ratio of singly ionized atoms to neutral:

$$\frac{N_1}{N_0} P_\mathrm{e} = \frac{(2\pi m_\mathrm{e})^{3/2} (kT)^{5/2}}{h^3} \frac{2u_1(T)}{u_0(T)} \mathrm{e}^{-I/kT} \tag{1.6}$$

where N_1 and N_0 are the number of singly ionized and neutral atoms respectively; P_e is the electron pressure; m_e is the electron mass; h is Planck's constant; u_1/u_0 is the ratio of ion to neutral atom partition functions, $u(T) = \sum g_i \mathrm{e}^{-\chi_i/kT}$; I is the ionization energy. Increasing temperature increases the ratio of higher levels being populated, to a certain point where ionization processes take over and dampen the higher level populations (Gray 2008).

1.3.2 Weak Line Approximation

Beyond affecting the quantum processes, temperature will affect the strength and shape of individual spectral lines. The line strength also changes with abundance; this relation is linear for what is known as "weak lines". Spectral lines have a Voigt profile, which is a convolution of a Lorentzian and Gaussian profile, and for weak lines the Gaussian core that occurs from Doppler broadening dominates the line profile.

These are the lines we use to determine temperature, however abundance must also be determined in parallel. We can see what parameters the line strengths of weak lines depend on through the Weak-Line Approximation:

$$\log\left(\frac{w}{\lambda}\right) = \log A + \log gf + \log C - \theta_\mathrm{ex}\chi - \kappa_\nu \tag{1.7}$$

Where w is the equivalent width of the line, defined as the width of a rectangle with area equal to the line with height of continuum emission; λ is the wavelength of the spectral line; A is the abundance of the element; C is a constant dependent on the ionization distribution of the element; gf is the statistical weight of a lower level g_l multiplied by the

oscillator strength of the transition $f_{\rm lu}$, dependent on Einstein coefficient of the transition (as $g_{\rm l}f_{\rm lu} = g_{\rm u}f_{\rm ul}$ this is simplified to just gf value); $\theta_{\rm ex}$ is correspondent to the inverse of the temperature, and χ is the excitation potential of the lower level; κ_ν^c is the continuum absorption coefficient (units of area per mass) for a given frequency; it describes losses in radiation through absorption and scattering processes that may remove photons / deviate their paths from the solid angle in consideration, and these processes are heavily affected by temperature. More details are provided in Gray (2008).

Thus, we now have some understanding of how temperature may affect spectral lines. We follow by different methods of temperature determination utilised in astronomy.

1.4 Methods of determining $T_{\rm eff}$

Several methods of determining stellar parameters are described in the recent review Jofre et al. (2019). We look at the various methods of effective temperature determination, and their pros and cons as found through research.

1.4.1 Infrared Flux Method (IRFM)

The infrared flux method is also known as photometric temperatures. Should stars have no atmosphere, they would act like perfect black bodies; a star's atmosphere absorbs some of the emitted light which is what gives us spectral lines. Treating a star like a black body, its spectrum will have a shape according to Wien's approximation, with a peak in brightness at a certain wavelength corresponding to the temperature (Gray 2008).

By looking at the brightness of stars in different wavelength bands and subtracting them, one obtains a "colour" (typically, this is B-V, blue and visible bands respectively). In IRFM, the ratio of measured bolometric flux to monochromatic flux on Earth is compared to that of the model of the surface of a star, each quotient being referred to as an R-factor as follows (Gonzalez Hernandez & Bonifacio 2009):

$$R_{\rm obs} = \frac{F_{\rm bol}(\text{Earth})}{F_{\lambda_{\rm IR}}(\text{Earth})} = \frac{\sigma T_{\rm eff}^4}{F_{\rm mod}(\lambda_{\rm IR}, T_{\rm eff}, [\text{Fe/H}], \log\, g)} = R_{\rm theo} \tag{1.8}$$

For stars hotter than M-type, the absorption processes occurring in the IR region of the spectrum are relatively small, meaning that in this region the flux of the star follows the black-body model quite well. This reduces the measurements to accurately determining $R_{\rm obs}$ which is done through photometry, allowing us to find a relation between colour and temperature. As this relation is linear for stars of certain spectral types, we can use the colour in a Hertzsprung-Russel diagram (as in Figure 1.2). If spectral class and approximate metallicity of a stellar sample is known, the temperature of other stars in the population can be determined from the HR-diagram (Jofre et al. 2019).

Casagrande et al. (2020) use this method, looking at wavelength bands in NIR and comparing the uncertainty of different colours used. The advantage of looking at the

spectra in NIR is that there the star is closest to a black body, giving the best model flux measurement.

Extinction is a big problem for this method, as interstellar reddening will make stars appear redder and thus cooler than they actually are. IFRM is also dependent on having good flux calibration; making sure that the continuum flux is correct, the calibration of which is dependent on multiple variables such as the telescope parameters and the light absorption of the Earth's atmosphere/interstellar media (Jofre et al. 2019).

1.4.2 Balmer line profile fitting

Balmer lines describe transitions in the hydrogen atom, and for FGK-type stars, the line strength (or equivalent width) of these lines is essentially only dependent on temperature. The strength of these lines in such spectra has made it a popular method, however it is also an indication that the lines were formed in the deeper layers, where convection becomes important. Because of this, we cannot use a typical 1D star model that we would use for other spectral lines. (Jofre et al. 2019)

This technique also depends on accurate continuum determination, something that can only be done for high-res, wide range spectra which is not always available. Amarsi et al. (2018) compare the difference between using traditional 1D versus 3D non-LTE models when looking at Balmer lines, and find a significant difference in the line width in the two cases, significantly improving the method and removing its largest source of uncertainty.

1.4.3 Interferometry

From the Steffan Boltzmann law in equation (1.3), we can find that the temperature can be determined if the bolometric flux, distance to the star, and its angular diameter is known. Inteferometry can be used to determine the sizes of stars; treating a star in the sky as an aperture in a screen, a diffraction pattern can be associated with it depending on its diameter and distance to Earth (Mozurkewich et al. 2003). This can only be done for closer stars, as stars far away have too small of an angular diameter in our sky.

Combining this with bolometric fluxes determined from surveys such as Gaia, this is one of the most accurate methods of $T_{\rm eff}$ determination. However, it is not without issues. It depends heavily on careful analysis of systematic errors in measurements (White et al. 2018). Limb darkening (the edges of stars showing higher, dimmer photospheric layers) which is dependent on stellar composition must also be accounted for, thus the method is not entirely model free.

1.4.4 Excitation balance

In lower layers of the atmosphere such as the photosphere, we assume local thermodynamic equilibrium (LTE) where collisions dominate the population mechanisms of atomic energy levels. When this is the case, the level populations can be described by Boltzmann statistics, shown in equation (1.5).

FGK-type stars typically have have their spectra populated most largely by Fe I spectral lines. The equivalent widths of Fe I lines are sensitive to an increase in $T_{\rm eff}$; this sensitivity changes depending on excitation energy. By requiring that abundances obtained are independent of the excitation energy, we can put a constraint on $T_{\rm eff}$ (Takeda et al. 2002). In metal-poor stars, other neutral elements that produce many lines can be used for the same method.

This method determines $T_{\rm eff}$ through spectral synthesis (explained in section 1.4.6), and it is particularly popular when analysing high-res spectra of cooler stars, as many neutral lines can be found. However, LTE cannot be applied to all spectral lines, inducing an error; Bensby et al. (2014) find a difference of $\sim$ 30 K upon applying non-LTE corrections.

1.4.5 Molecular Band heads

Molecules can also produce spectral lines, though the mechanisms behind it are more complex than for single atoms. Relative movements of atoms within the molecule (whether vibrational or rotational) create many more energy states slightly above each electronic state. Because of this, molecules produce many absorption lines with minuscule energy differences. Groups of lines for certain transitions form spectral bands. The lines pile up at the edge of these regions forming what is known as a band head.

The temperature determination using molecular band heads is dependent on equivalent widths. Schultheis et al. (2016) find a tight relation between $T_{\rm eff}$ and the equivalent width of various CO band heads. It has been shown that this relation holds for low-res spectra with resolution power of $\sim$ 2000, and within their uncertainty of 200 K is essentially independent of metallicity for M-Giants making it viable when high-res spectra are not available.

1.4.6 Spectral synthesis

In this thesis, we utilise excitation balance and molecular bands in combination with spectral synthesis. Spectral synthesis works through creating synthetic spectra from given stellar parameters, and altering the parameters until the spectral synthesis best fits an observed spectrum. There are different ways this is done.

The spectral synthesis method used in this thesis as well as in Jönnson et. al. (in prep.) is through code named Spectroscopy Made Easy (SME), which produces an initial synthetic spectrum, and then iteratively improves the fit of the synthetic spectrum by altering free parameters (Valenti & Piskunov (1996), Piskunov & Valenti (2017)).

An alternate method of finding abundances creates a grid of synthetic spectra for all possible parameters, and with interpolation the best match is picked for an observed spectrum. The APOGEE Stellar Parameters and Chemical Abundances Pipeline (ASPCAP) is utilized with this method in Holtzman et al. (2015).

Spectral synthesis has an advantage of being able to handle line blending which is common in red giants; for the equivalent-width method such lines cause an overestimation in abundances. While the grid method of synthesis is faster, the method of iteration used in SME provides better accuracy (Blanco-Cuaresma 2019).

Chapter 2

Method

Temperature determination for our stellar sample was done through spectral line synthesis using SME, inputting a starting temperature between 4000 K and 5100 K with intervals of 100 K and starting metallicity of 0.00 dex. The other stellar parameters input are taken from Jönsson et. al. (in prep). A variety of spectral line lists were used. The determined temperatures were then compared to those found in Jönsson et. al. (in prep) to examine which line list is most effective. The stellar sample, spectral line synthesis, and line lists are discussed in the sections below.

2.1 Stellar Sample

For our sample, red giants were used which are specifically favorable to observe in stellar spectroscopy as discussed previously. Their brightness allows for a high signal-to-noise ratio in their spectra even at large distances which makes them good probes. K-giants specifically are studied in this thesis, as they have all the previously described benefits, and are warm enough to minimise molecular crowding in infrared spectra.

A sample of 12 K-giants with a range of temperatures (4100 – 5200 K) and metallicities (-0.80 – 0.3 dex) has been selected to study, a subset of the sample studied in Jönsson et al. (in prep.). The stars were observed with the Lowell Discovery Telescope with the Immersion Grating Infrared Spectrometer (IGRINS) over a period of time 2019–2021 (PI: Ryde).

The temperatures determined by Jönsson et. al. (in prep) from spectral lines in the optical range were benchmarked against temperatures fundamentally determined from angular diameter, and are found to be very accurate and precise. They are among the best available and therefore are a good choice of benchmark. We take other stellar parameters from Jönsson et. al. (in prep) also, which can be seen in Table 2.1. The methods of temperature determination are similar between this thesis and the one used by Jönnson et. al. (in prep.), allowing to compare the effectiveness of lines used typically in the optical range against those available in the IR. A comparison of the observational differences are shown in Table 2.2.

Table 2.1: Selection of stars used for analysis

Name of Star	T_{eff} [K]	[Fe/H]
Arcturus	4308	-0.56
Epsilon Virginis	5112	0.15
μLeo	4494	0.23
HIP 96014	4240	-0.35
KIC 3955590	4411	0.06
KIC 5113061	4100	-0.08
KIC 5859492	4511	0.14
KIC 6547007	4738	-0.72
KIC 6465075	4825	-0.28
KIC 11444313	4630	-0.09
HD102328 K3III	4442	0.30
HD142091 K0III-IV	4845	0.06

Table 2.2: Comparison of the observations of the stellar populations

Study	This Thesis	Jönnson
Spectrograph	IGRINS	FIES
Wavelength region	15000 - 18000 Å	3700 - 8300 Å
Resolving power	45000	67000

2.2 Line synthesis

In this thesis, the line synthesis method is used through code named Spectroscopy Made Easy (SME). SME uses stellar parameters in the form of atmospheric models and atomic data to model how light would pass through a star's photosphere, synthesising a spectrum (Valenti & Piskunov (1996), Piskunov & Valenti (2017)). Stellar parameters are input allowing to select a model of the atmosphere, and certain parameters can be set free (in this case, T_{eff} and [Fe/H]). The synthetic spectrum is matched to an observed one by altering the parameters over several iterations, minimising the difference χ^2 between the spectra until the best match is found.

To save time in modelling and calculation of the synthetic spectra, only certain parts of the spectrum are used in the process. Line-dense segments of the spectrum are selected, in which spectral lines and surrounding continuum are identified, an example of this is shown in Figure 2.1.

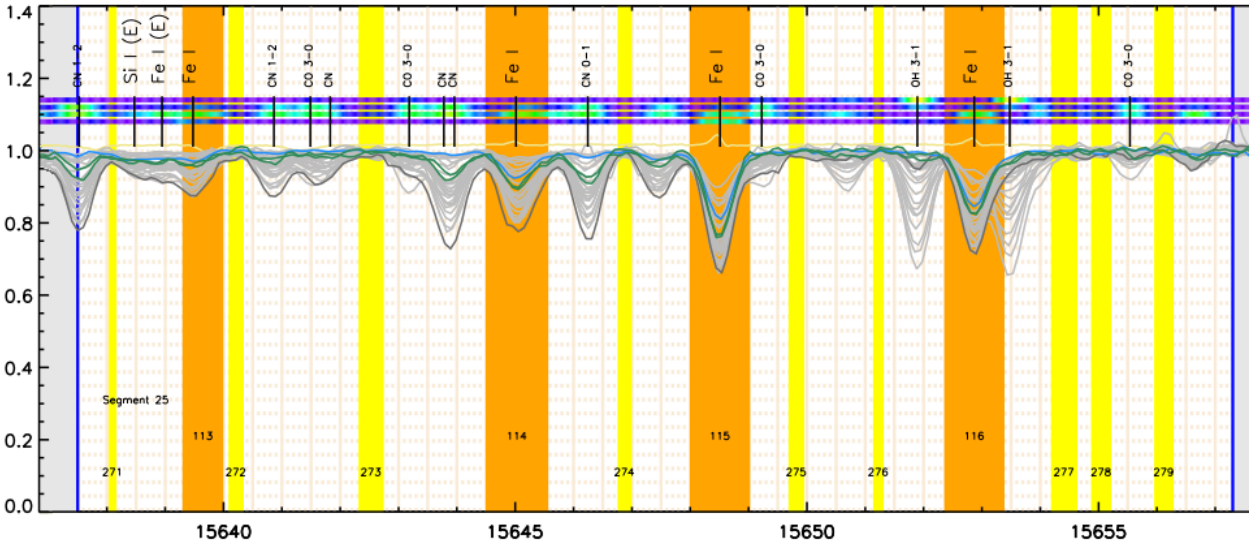

Figure 2.1: Small segment of stellar spectra, showing several Fe I iron spectral lines. The x-axis shows the wavelength in [Å], while the y-axis displays relative flux. The spectra are normalised to 1 at continuum. The orange segments mark lines we wish to look at, while the yellow segments are continuum for comparison. The grey spectra are spectra of several stars which include the sample used in this thesis. Other spectra are highlighted, such as the blue spectrum (the Sun), the dark grey spectrum (metal rich μLeo). The light yellow spectrum shows the telluric spectrum, produced by molecules in the Earth's atmosphere which has been divided out of the stellar spectra as well as possible.

2.3 Model Atmospheres

To be able to synthesize a spectrum, we need a model of the photosphere that approximates the physical conditions of a stellar atmosphere. The models utilized with SME are MARCS model atmospheres which use several assumptions (Gustafsson et al. 2008):

- Local thermodynamic equilibrium; the concept of thermodynamic equilibrium where no energy escapes or enters a system doesn't describe a star overall well as it is constantly releasing large amounts of energy. However, by *local* thermodynamic equilibrium we assume that energy changes in the system are slow enough that the temperatures of individual particles are dominated by collisions (Gray 2008).

- Hydrostatic equilibrium; the hydrostatic equilibrium equation provides the pressure structure of the atmosphere. The forces of gravity and pressure are assumed to balance each-other out.

- Spherical symmetry; when modelling atmospheres it can typically be enough to use plane parallel geometry, wherein physical variables only depend on the vertical depth. Such models work well for dwarves, however for atmospheres that are thicker in

comparison to the stellar radius, such as those in giants, we must also account for the curvature through spherical symmetry.

2.4 Linelists

To identify spectral lines to use in the spectra synthesis, a line list must first be provided that aggregates essential information about each line. This information includes:

- Chemical element and its ionization level
- Wavelength of the line
- Lower and upper excitation potential
- gf value of the transition (product of statistical weight g and oscillator strength f)
- Broadening parameters, most importantly van der Waals

The line lists used in this thesis are discussed next.

2.4.1 Fe I

The Fe I line list used in this thesis are provided by Montelius (2021). The basis of the line list is the Vienna atomic line database (VALD), that collects a large assortment of information about each line such as wavelength, excitation energy, full descriptions of electronic configurations and others from a variety of sources (Ryabchikova et al. 2015). Montelius (2021) improves the line list with additions from literature sources and observational measurements such as van der Waals broadening, and supplements with empirical determinations of gf values for transitions that previously did not have these measured.

A subset of the relatively stronger lines was initially used for parameter determination, and then increased to a longer line list. Line blending with other atoms and molecules was avoided as best as possible by using line lists to indicate where they would occur on the spectrum (see Figure 2.1, many lines are labelled but only Fe I lines with no clear blending were chosen), as these would skew the calculation of the equivalent width.

2.5 CO

The addition of CO lines and band heads was also explored in this thesis, as their equivalent widths show a strong correlation to T_{eff} (e.g. Schultheis et al. (2016)). The CO line list used is from Goorvitch (1994), line masks were created for the CO lines and band heads most prominent in the spectra. These were used in combination with the Fe I line list, as well as individually.

Chapter 3

Results & Discussion

The results are presented and discussed in this section. For each line list used for temperature determination a plot displays the temperature determined in this thesis from lines in IR range, against our benchmark, determined in the optical range in Jönnson et. al. (in prep.). The metallicity of each star from Jönnson et. al. (in prep.) is highlighted to see how it may affect results. The grey dashed line in the figures is a one-to-one. The black dash-dot lines are lines of best fit of the determined temperatures.

As the starting temperatures affected the resulting temperatures (see Table 3.1 showing an example of KIC5859492) the final $T_{\rm eff}$ is taken to be an average of them all for each star.

Table 3.1: Resulting temperatures $T_{\rm eff}^{\rm end}$ for different starting temperatures $T_{\rm eff}^{\rm start}$ for KIC5859492 of nominal temperature 4511 K for combined Fe I and CO line list. The mean is 4531 K

$T_{\rm eff}^{\rm start}$	4000	4100	4200	4300	4400	4500	4600	4700	4800	4900	5000	5100
$T_{\rm eff}^{\rm end}$	4532	4527	4529	4531	4524	4529	4530	4533	4534	4535	4535	4534

3.1 Fe line lists

We started with two different Fe I line lists: the first containing ∼10 lines, and the second containing ∼60 lines. The resulting $T_{\rm eff}$ found from the short and long Fe I line list can be seen in Figure 3.1. For the short line list, the difference between determined $T_{\rm eff}$ and the benchmark is small for the lower temperatures, however gets greater as the star temperatures get hotter. The longer line list however seems to give consistently cooler temperatures than what we are expecting and the determined temperatures are more spread out, with an rms of 242.4 K for the short line list and 297.0 K for the longer line list.

In the temperatures determined by both Fe I line lists a consistent outlier is Epsilon Virginis, which has a $T_{\rm eff}$ of $\sim$ 5100 K. This is possibly due to it being at the limit in the

range of temperatures that can be determined using this method.

If there is not a large enough range of excitation potentials in selected lines, the temperatures determined from them may still be excitation potential dependent. A comparison of the excitation potential of Fe I lines used in the optical range and infrared can be seen in Figure 3.2. Because of this, one would expect similarly accurate results in the temperatures determined; there is an equally wide range of excitation potentials for SME to fit to, removing possible excitation potential dependence that a smaller range of lines would have. However, this is not the case.

A potential reason for poor results by using iron lines in the IR range compared to optical may be found when assessing line strength dependence on excitation potential and temperature. This is done in Gray (2008) giving the following equation for a "weak" neutral line from a mostly ionized element (which is the case for Fe I in the Sun);

$$\frac{1}{R}\frac{\mathrm{d}R}{\mathrm{d}T} = \frac{\chi + 0.75 - I}{kT^2}.$$

Here, $R = \kappa_\nu^l/\kappa_\nu^c$ is the ratio of line to continuous absorption at a given frequency ν, which is directly related to line strength;K χ is the excitation potential of a lower level; I is the ionization potential ($\sim$7.9 eV for Fe I); T is the temperature; k is the Boltzmann constant. For a given temperature, an increase in the excitation potential χ decreases the change in R for the same change in T meaning that the line strength of higher excitation potentials is relatively less sensitive to temperature than that of lines with low excitation potential.

As seen in Figure 3.2, the Fe I lines used in the optical range for temperature determination are in a lower range of excitation potentials ($\sim$3.5 – 5.3 eV) than the ones used in this thesis ($\sim$ 5.3 – 6.6 eV). As SME iterates temperatures until the synthetic and observed lines match, having lines that are less sensitive to temperature will produce worse results.

A majority of the lines used in the longer line list have excitation potentials >6 eV, which may explain the larger scatter of resulting temperatures as SME works to provide the best overall fit and these lines would be relatively less temperature sensitive.

Due to the relatively poor results, we then chose to look at T_{eff} determined from CO lines in the same range of wavelengths, the results of which are discussed next.

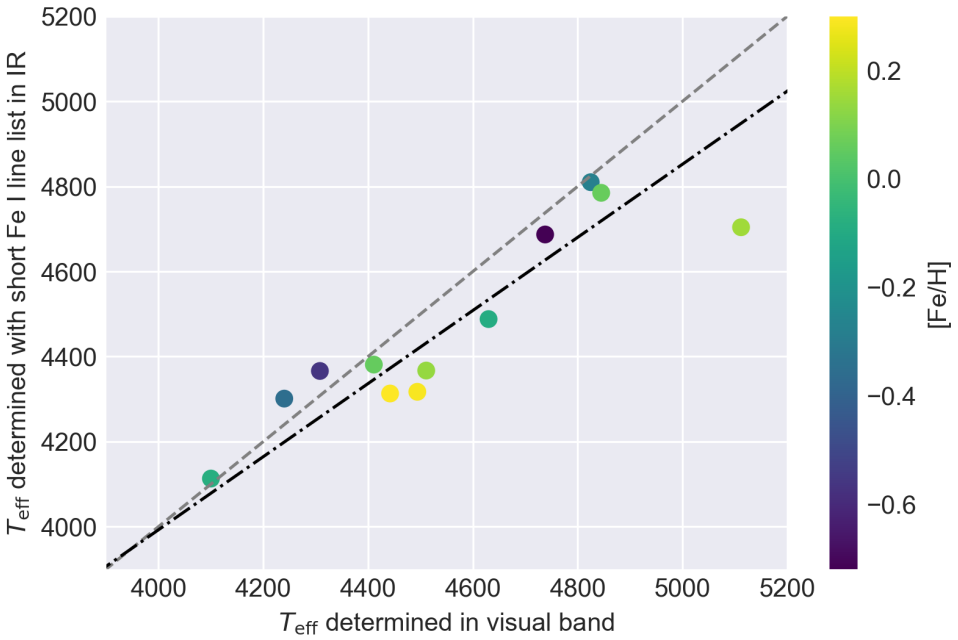

(a) Short Fe I line list of 10 lines

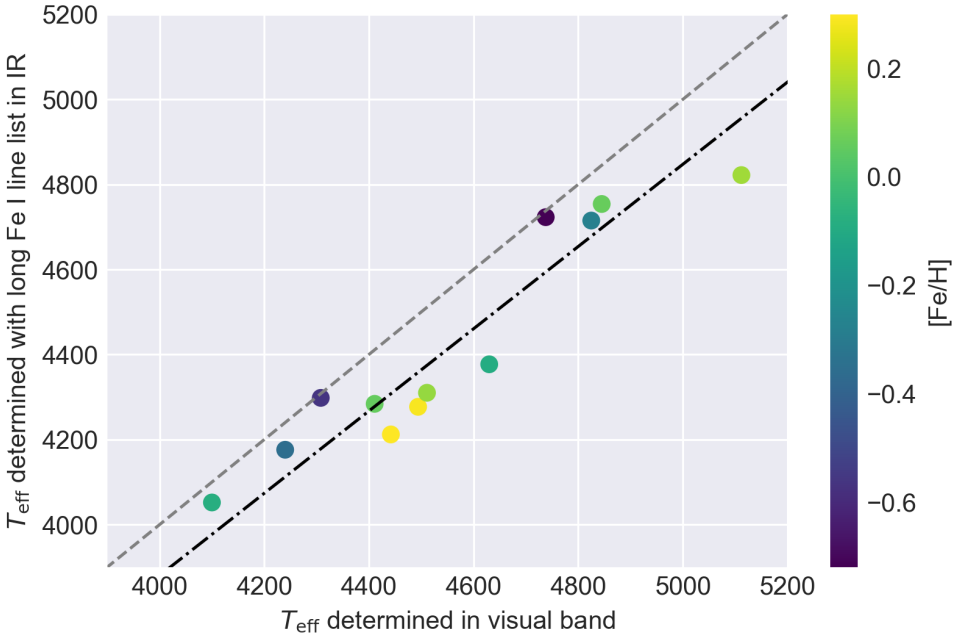

(a) Long Fe I line list of ∼60 lines

Figure 3.1: A comparison of $T_{\rm eff}$ determined in the optical range to that in IR, using different amounts of Fe I lines. A color bar shows the optical metallicity of each star. The grey line is a diagonal. The black line is the line of best fit of the determined temperatures

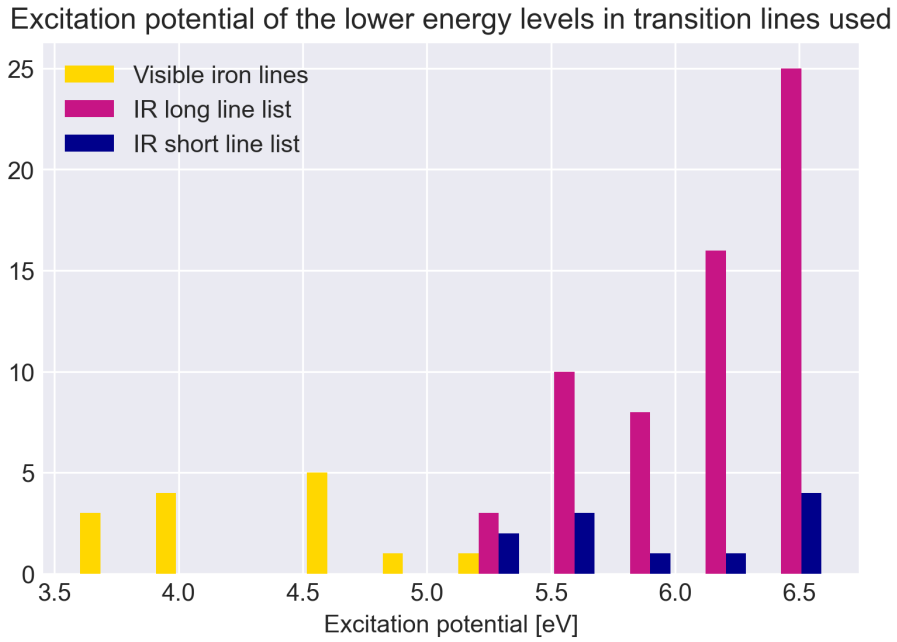

Figure 3.2: Excitation potentials of the lower levels for the different Fe I line lists used in temperature determination

3.2 CO linelist

The temperature determined using CO lines and bandheads compared to our benchmark can be seen in Figure 3.3. On its own, the CO line list produces temperatures closer to the benchmark than the Fe I line lists, with an rms from the line of best fit of 122 K. However it is necessary to note that the abundances of C, O and N were set to be those determined in the benchmark.

There are several outliers here. Epsilon Virginis is the highest in temperature and at greater temperatures the CO lines become weaker. Stars with metallicity >0.2 dex also stand out; the reason for their poor temperature determination is unclear, it could be possible that there is an increase in line blending with other molecules or atoms, producing a fit that gives incorrect parameters. KIC11444313 stands out as being further from the fit than the other stars, however the reason for this is unclear as it is not in the extremes of either metallicity or temperature.

A factor worth considering is that the temperature sensitivity of CO bandheads found in Schultheis et al. (2016) is found for much lower resolution spectra (R $\sim$ 2000) than those used in this thesis, for M-giants which are also cooler. The cooler stars have stronger lines, and lower-resolution blends the individual molecular lines and allow to find consistent continuum points easier for different stars. It is possible that the continuum determined in high-res could be different from the continuum in low-res and thus introduce an offset.

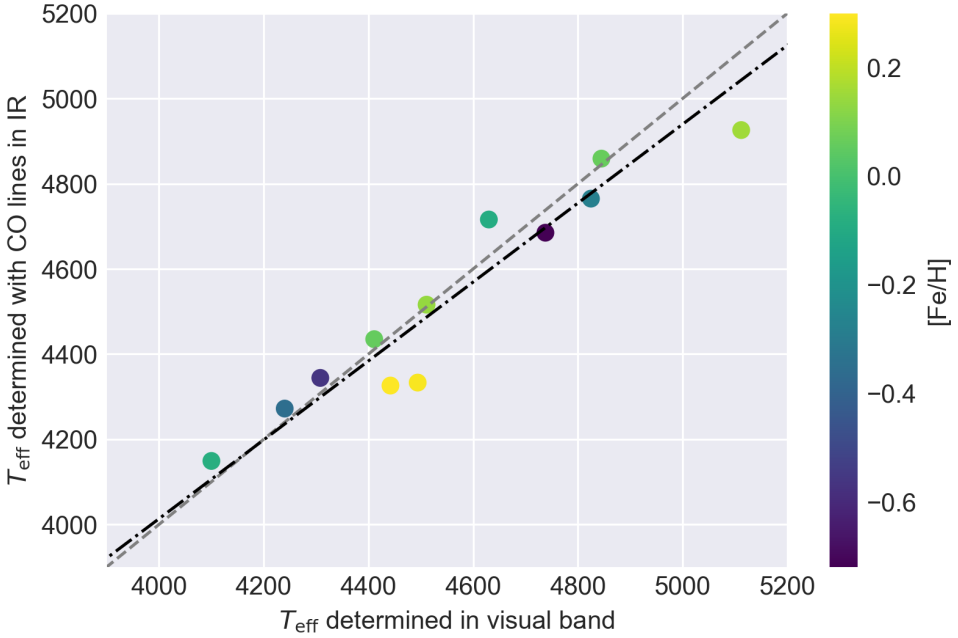

Figure 3.3: A comparison of $T_{\rm eff}$ determined using CO molecular lines and band heads to the temperature determined from Fe I lines in the optical range (Refer to Figure 3.1 for details).

3.3 CO and Fe I line combined list

To see if the results could be improved, the CO line list was combined with the long Fe I line list for a final temperature determination. The results are shown in Figure 3.4. This run produced the closest temperatures to the benchmark, with an rms of 88 K, showing that a combination of CO and Fe I lines give results comparable to those found in the optical range with only Fe I lines.

The temperatures determined this way seem to be slightly hotter than the benchmark, with the exception of μLeo and HD102328 K3III which are notably higher in metallicity than the other stars in the sample, and Epsilon Virginis which is hotter than the other stars in the sample.

With the exclusion of these outliers, the temperatures determined in IR with the combined Fe I and CO list and those determined in the optical range are on average 44 K hotter with a standard deviation σ =24 K in the difference. This is however, with the use of high resolution spectra and known C, N and O abundances. There are no obvious outliers in the metallicity determined, these are on average 0.01 dex lower than the benchmark with $\sigma = 0.04$ dex.

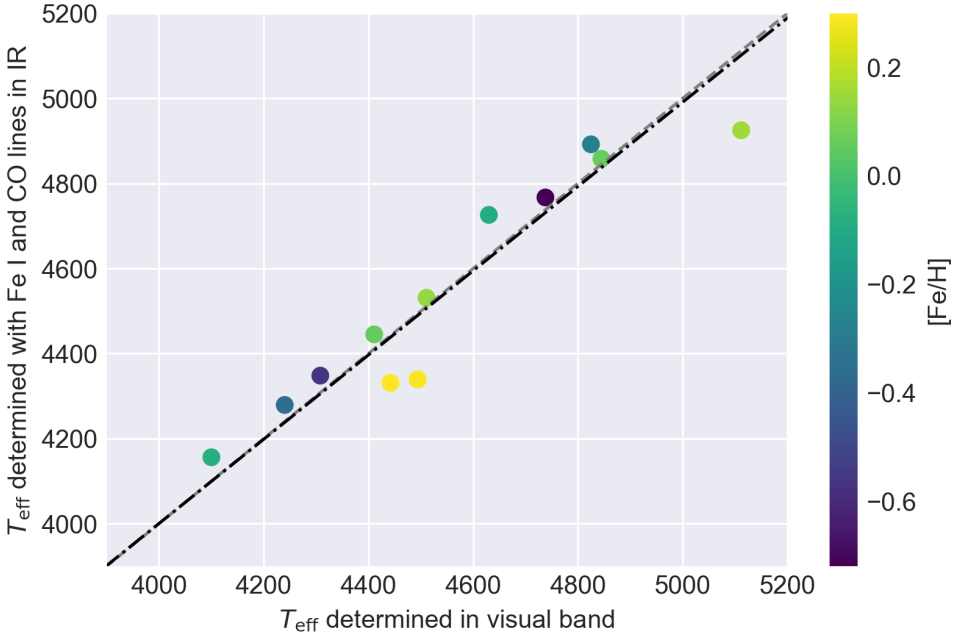

Figure 3.4: A comparison of $T_{\rm eff}$ determined using a combination of the CO and long Fe I line lists, and the temperature determined from Fe I lines in the optical range (Refer to Figure 3.1 for details). The line of best fit has a slope of 1.001 and intercept of -38.6 K.

Table 3.2: Selection of stars used for analysis

Name of Star	$T_{\rm eff}^{\rm Optical}$ [K]	$[{\rm Fe/H}]_{\rm Optical}$	$T_{\rm eff}^{\rm IR}$ [K]	$[{\rm Fe/H}]_{\rm IR}$	$\Delta T_{\rm eff}$ [K]	$\Delta[Fe/H]$
Arcturus	4308	-0.56	4348	-0.54	40	0.03
μLeo	4494	0.29	4339	0.27	-155	-0.02
Epsilon Virginis	5112	0.15	4925	0.07	-187	-0.08
HIP 96014	4240	-0.35	4279	-0.35	39	-0.01
KIC 3955590	4411	0.06	4445	0.05	34	-0.01
KIC 5113061	4100	-0.08	4156	-0.13	56	-0.05
KIC 5859492	4511	0.14	4531	0.13	20	-0.01
KIC 6465075	4825	-0.28	4767	-0.30	67	-0.02
KIC 6547007	4738	-0.72	4892	-0.65	29	0.07
KIC 11444313	4630	-0.09	4726	-0.09	96	0.01
HD102328 K3III	4442	0.30	4331	0.28	-111	-0.02
HD142091 K0III-IV	4845	0.06	4858	0.10	13	0.04

Chapter 4

Conclusion

The aim of this thesis was to explore effective temperature determination of K giants through spectral line synthesis in the infrared, and compare it to results determined from spectra in the optical range.

We found that for effective temperature determination in infrared, it is not enough to use only Fe I lines as done in the optical range; in the infrared range these have higher excitation energies than in optical, which makes the spectral lines less sensitive to temperature. CO molecular lines and band heads alone provided better results, however the best results were found from a combination of Fe I and CO lines, that on average gave temperatures 40 K higher than in optical. These results are found with C, N and O abundances pre-determined in the optical range; the infrared determinations of these are out of the scope of this thesis.

There are limitations to this method, as seen for stars with [Fe/H] >0.2 dex and temperatures greater than 5000 K. Future research could determine the effect of metallicity on the temperature determination using CO lines, as well as exploring whether using the combination of Fe I and CO lines produces just as good results in lower resolution or lower signal-to-noise ratio spectra than the spectra used here.

Bibliography

Amarsi, A. M., Nordlander, T., Barklem, P. S., et al. 2018, Astronomy Astrophysics, 615, A139

Bensby, T., Feltzing, S., & Oey, M. S. 2014, Astronomy Astrophysics, 562, A71

Blanco-Cuaresma, S. 2019, Monthly Notices of the Royal Astronomical Society, 486, 2075

Casagrande, L., Lin, J., Rains, A. D., et al. 2020

Fraunhofer, J. 1815, Memoirs of the Royal Academy of Sciences in Munich, 5, 193

Gonzalez Hernandez, J. I. & Bonifacio, P. 2009, Astronomy Astrophysics, 497, 497

Goorvitch, D. 1994, The Astrophysical Journal Supplement Series, 95, 535

Gray, D. F. 2008, The Observation and Analysis of Stellar Photospheres (Cambridge: Cambridge University Press)

Gustafsson, B., Edvardsson, B., Eriksson, K., et al. 2008, Astronomy Astrophysics, 486, 951

Harrison, K. M. 2011, Astronomical spectroscopy for amateurs (Springer)

Holtzman, J. A., Shetrone, M., Johnson, J. A., et al. 2015, The Astronomical Journal, 150, 148

Horiba. 2021, Introduction to the detectors techniques, `https://www.horiba.com/en_en/technology/measurement-and-control-techniques/spectroscopy/detectors/detectors/`, [Accessed: 04/05/2021]

Jofre, P., Heiter, U., & Soubiran, C. 2019, Annual Review of Astronomy and Astrophysics, 57, 571

Jönsson, H., Ryde, N., Nordlander, T., et al. 2017, Astronomy Astrophysics, 598, A100

Longshore, R. E. 2002, Handbook of Infra-red Detection Technologies, 233

Masseron, T. 2015, 303

Matteucci, F. 2001, The chemical evolution of the galaxy (Kluwer Academic Publishers)

Montelius, M. 2021, Master's thesis, Lund

Mozurkewich, D., Armstrong, J. T., Hindsley, R. B., et al. 2003, The Astronomical Journal, 126, 2502

Piskunov, N. & Valenti, J. A. 2017, A&A, 597, A16

Rieke, G. H. 2009, Experimental Astronomy, 25, 125

Ryabchikova, T., Piskunov, N., Kurucz, R. L., et al. 2015, Physica Scripta, 90, 054005

Schultheis, M., Ryde, N., & Nandakumar, G. 2016, Astronomy Astrophysics, 590, A6

Takeda, Y., Ohkubo, M., & Sadakane, K. 2002, Publications of the Astronomical Society of Japan, 54, 451

Valenti, J. A. & Piskunov, N. 1996, , 118, 595

White, T. R., Huber, D., Mann, A. W., et al. 2018, Monthly Notices of the Royal Astronomical Society, 477, 4403

Appendix A

Fe I short line list tables of results

In the following appendices, tables of the temperatures and metallicites determined for each starting temperature of each line list are shown. A histogram of the differences in determined and benchmark temperatures for all runs are shown for for each line list.

Table A.1: $T_{\rm eff}$ in units of Kelvin determined from short Fe I line list for different starting temperatures

	4000	4100	4200	4300	4400	4500	4600	4700	4800	4900	5000	5100
ABOO	4367	4367	4367	4367	4367	4367	4367	4363	4366	4365	4366	4367
muLeo	4333	4287	4300	4303	4302	4303	4318	4334	4335	4331	4331	4331
EpsVir	4619	4611	4592	4617	4612	4659	4714	4768	4808	4818	4817	4817
HIP96014	4300	4301	4301	4301	4301	4301	4301	4301	4301	4301	4301	4305
KIC3955590	4373	4362	4370	4375	4381	4386	4390	4388	4388	4388	4388	4389
KIC5113061	4114	4115	4115	4115	4115	4120	4112	4115	4119	4107	4101	4117
KIC5859492	4365	4350	4359	4364	4366	4365	4370	4361	4381	4375	4375	4375
KIC6465075	4809	4585	4573	4592	4630	4698	4804	4916	4982	5041	5047	5045
KIC6547007	4681	4682	4682	4682	4682	4692	4690	4695	4690	4700	4689	4691
KIC11444313	4463	4443	4467	4479	4503	4503	4501	4502	4501	4502	4502	4500
HD102328_K3III	4307	4297	4310	4312	4310	4309	4310	4315	4320	4326	4325	4326
HD142091_K0III-IV	4780	4742	4790	4740	4724	4743	4744	4737	4798	4837	4876	4915

Table A.2: [Fe/H] in units of dex determined from short Fe I line list for different starting temperatures

	4000	4100	4200	4300	4400	4500	4600	4700	4800	4900	5000	5100
ABOO	-0.52	-0.52	-0.52	-0.52	-0.52	-0.52	-0.52	-0.52	-0.52	-0.52	-0.52	-0.52
muLeo	0.28	0.26	0.26	0.26	0.26	0.26	0.27	0.27	0.28	0.28	0.28	0.28
EpsVir	-0.10	-0.10	-0.11	-0.10	-0.10	-0.08	-0.05	-0.03	-0.01	0.00	0.00	0.00
HIP96014	-0.32	-0.32	-0.32	-0.32	-0.32	-0.32	-0.32	-0.32	-0.32	-0.32	-0.32	-0.32
KIC3955590	0.07	0.06	0.06	0.06	0.07	0.07	0.07	0.07	0.07	0.07	0.07	0.07
KIC5113061	-0.08	-0.08	-0.08	-0.08	-0.08	-0.09	-0.09	-0.08	-0.08	-0.08	-0.09	-0.08
KIC5859492	0.11	0.10	0.11	0.11	0.11	0.11	0.11	0.11	0.11	0.12	0.12	0.12
KIC6465075	-0.27	-0.38	-0.38	-0.37	-0.36	-0.33	-0.27	-0.21	-0.17	-0.13	-0.13	-0.13
KIC6547007	-0.73	-0.73	-0.73	-0.73	-0.73	-0.72	-0.73	-0.72	-0.73	-0.72	-0.73	-0.72
KIC11444313	-0.13	-0.14	-0.13	-0.12	-0.11	-0.11	-0.11	-0.11	-0.11	-0.11	-0.11	-0.11
HD102328_K3III	0.27	0.27	0.27	0.27	0.27	0.27	0.27	0.27	0.28	0.28	0.28	0.28
HD142091_K0III-IV	0.06	0.04	0.08	0.05	0.03	0.05	0.05	0.04	0.08	0.10	0.12	0.14

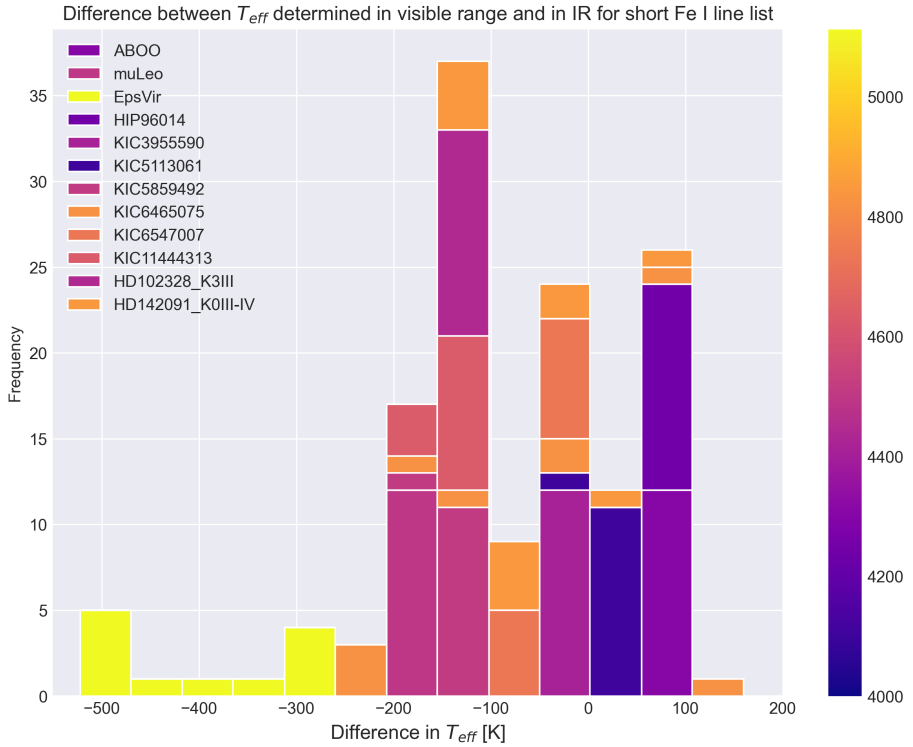

Figure A.1: Difference in $T_{\rm eff}$ between determined value and benchmark for short Fe I line list

Appendix B

Fe I long line list results

Table B.1: $T_{\rm eff}$ in units of Kelvin determined from long Fe I line list for different starting temperatures

	4000	4100	4200	4300	4400	4500	4600	4700	4800	4900	5000	5100
ABOO	4297	4295	4298	4298	4299	4298	4299	4299	4299	4299	4300	4299
muLeo	4278	4276	4275	4276	4276	4276	4277	4277	4278	4281	4278	4278
EpsVir	4929	4937	4756	4748	4758	4758	4747	4750	4804	4880	4954	4981
HIP96014	4177	4178	4174	4174	4174	4175	4177	4178	4175	4178	4200	4179
KIC3955590	4284	4283	4282	4285	4285	4285	4285	4285	4285	4285	4323	4285
KIC5113061	4042	4042	4054	4056	4056	4054	4056	4054	4056	4055	4155	4055
KIC5859492	4324	4326	4306	4306	4307	4307	4307	4307	4307	4308	4367	4307
KIC6465075	4693	4651	4657	4663	4651	4658	4694	4722	4721	4719	4677	5045
KIC6547007	4818	4840	4697	4697	4698	4696	4701	4702	4701	4703	4432	4702
KIC11444313	4389	4391	4373	4374	4374	4374	4374	4376	4377	4375	4722	4373
HD102328_K3III	4218	4217	4211	4211	4211	4211	4211	4210	4210	4211	4276	4213
HD142091_K0III-IV	4772	4773	4752	4745	4749	4738	4750	4745	4751	4759	4871	4761

Table B.2: [Fe/H] in units of dex determined from long Fe I line list for different starting temperatures

	4000	4100	4200	4300	4400	4500	4600	4700	4800	4900	5000	5100
ABOO	-0.55	-0.55	-0.52	-0.52	-0.52	-0.52	-0.52	-0.52	-0.52	-0.52	-0.52	-0.52
muLeo	0.27	0.27	0.27	0.27	0.27	0.27	0.27	0.27	0.27	0.27	0.27	0.27
EpsVir	0.06	0.06	0.00	0.00	0.00	0.00	0.00	0.00	0.02	0.05	0.10	0.10
HIP96014	-0.37	-0.37	-0.35	-0.35	-0.35	-0.35	-0.36	-0.36	-0.35	-0.36	-0.35	-0.36
KIC3955590	0.03	0.03	0.05	0.05	0.05	0.05	0.05	0.05	0.05	0.05	0.05	0.05
KIC5113061	-0.09	-0.09	-0.08	-0.08	-0.08	-0.08	-0.08	-0.08	-0.08	-0.08	-0.13	-0.08
KIC5859492	0.08	0.08	0.10	0.10	0.10	0.10	0.10	0.10	0.10	0.10	0.11	0.10
KIC6465075	-0.33	-0.35	-0.35	-0.35	-0.35	-0.35	-0.33	-0.32	-0.32	-0.32	-0.74	-0.13
KIC6547007	-0.70	-0.68	-0.73	-0.73	-0.73	-0.73	-0.73	-0.73	-0.73	-0.73	-0.13	-0.73
KIC11444313	-0.16	-0.16	-0.15	-0.15	-0.15	-0.15	-0.15	-0.15	-0.15	-0.15	-0.32	-0.15
HD102328_K3III	0.25	0.25	0.27	0.27	0.26	0.26	0.26	0.27	0.27	0.27	0.28	0.27
HD142091_K0III-IV	0.06	0.06	0.07	0.07	0.07	0.06	0.07	0.06	0.07	0.07	0.12	0.07

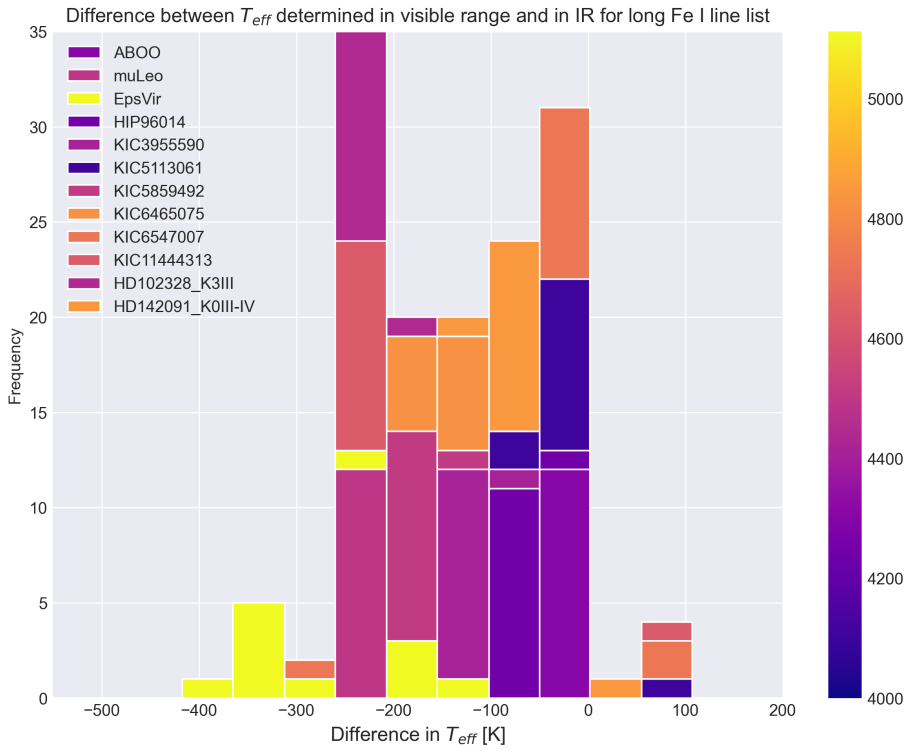

Figure B.1: Difference in $T_{\rm eff}$ between determined value and benchmark for long Fe I line list

Appendix C

CO line list results

Table C.1: $T_{\rm eff}$ in units of Kelvin determined from CO line list for different starting temperatures

	4000	4100	4200	4300	4400	4500	4600	4700	4800	4900	5000	5100
ABOO	4349	4349	4349	4349	4348	4349	4348	4348	4349	4349	4300	4349
muLeo	4353	4353	4353	4351	4351	4276	4353	4350	4350	4351	4278	4278
EpsVir	4961	4937	4902	4917	4932	4904	4920	4892	4916	4915	4954	4965
HIP96014	4278	4279	4279	4279	4279	4279	4280	4279	4279	4279	4200	4279
KIC3955590	4444	4446	4444	4445	4446	4445	4447	4445	4446	4446	4323	4446
KIC5113061	4169	4155	4155	4155	4155	4155	4155	4155	4155	4156	4078	4156
KIC5859492	4532	4527	4529	4531	4524	4529	4530	4533	4534	4535	4367	4534
KIC6465075	4796	4797	4797	4797	4796	4655	4797	4798	4798	4800	4677	4681
KIC6547007	4697	4709	4710	4698	4706	4709	4708	4714	4714	4715	4432	4714
KIC11444313	4693	4651	4657	4663	4651	4658	4694	4722	4721	4719	4722	5045
HD102328_K3III	4332	4332	4331	4331	4331	4331	4331	4331	4331	4331	4276	4330
HD142091_K0III-IV	4853	4855	4857	4858	4861	4854	4858	4861	4862	4854	4871	4866

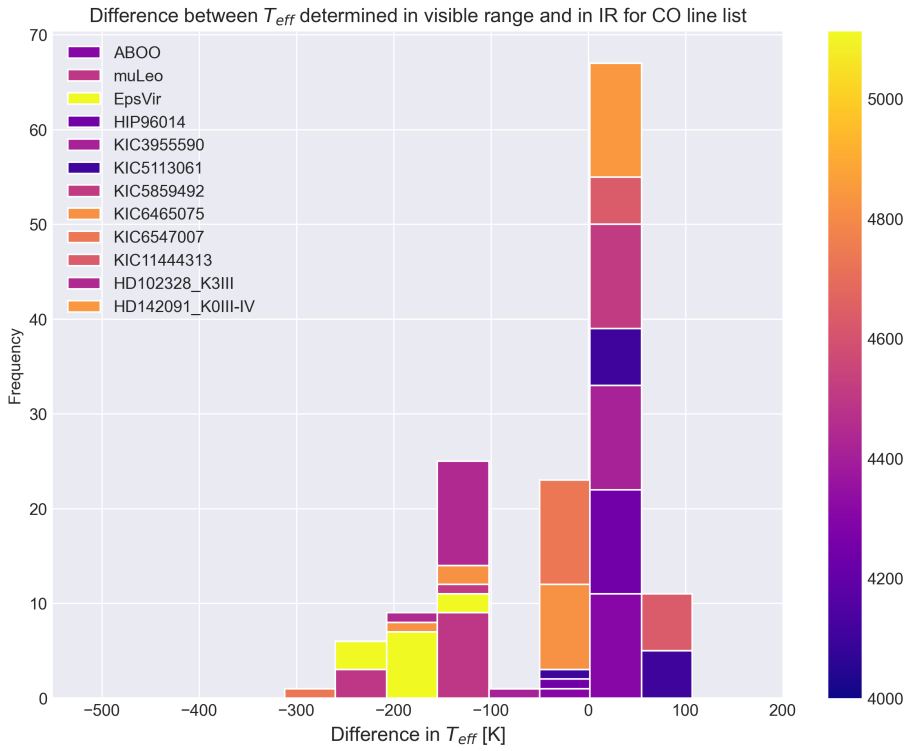

Figure C.1: Difference in T_{eff} between determined value and benchmark for CO line list

Appendix D

Fe I and CO line list tables of results

Table D.1: $T_{\rm eff}$ in units of Kelvin determined from combined Fe I and CO line list for different starting temperatures

	4000	4100	4200	4300	4400	4500	4600	4700	4800	4900	5000	5100
ABOO	4349	4349	4349	4349	4348	4349	4348	4348	4349	4349	4349	4349
muLeo	4353	4353	4353	4351	4351	4276	4353	4350	4350	4351	4351	4278
EpsVir	4961	4937	4902	4917	4932	4904	4920	4892	4916	4915	4944	4965
HIP96014	4278	4279	4279	4279	4279	4279	4280	4279	4279	4279	4279	4279
KIC3955590	4444	4446	4444	4445	4446	4445	4447	4445	4446	4446	4446	4446
KIC5113061	4169	4155	4155	4155	4155	4155	4155	4155	4155	4156	4155	4156
KIC5859492	4532	4527	4529	4531	4524	4529	4530	4533	4534	4535	4535	4534
KIC6465075	4907	4900	4901	4797	4889	4899	4899	4887	4903	4907	4909	4911
KIC6547007	4796	4797	4797	4698	4796	4655	4797	4798	4798	4800	4802	4681
KIC11444313	4697	4709	4710	4901	4706	4709	4708	4714	4714	4715	4716	4714
HD102328_K3III	4332	4332	4331	4331	4331	4331	4331	4331	4331	4331	4331	4330
HD142091_K0III-IV	4853	4855	4857	4858	4861	4854	4858	4861	4862	4854	4859	4866

Table D.2: [Fe/H] in units of dex determined from combined Fe I and CO line list for different starting temperatures

	4000	4100	4200	4300	4400	4500	4600	4700	4800	4900	5000	5100
ABOO	-0.54	-0.54	-0.54	-0.54	-0.54	-0.54	-0.54	-0.54	-0.54	-0.54	-0.54	-0.54
muLeo	0.27	0.27	0.27	0.27	0.27	0.27	0.27	0.27	0.27	0.27	0.27	0.27
EpsVir	0.10	0.08	0.06	0.07	0.07	0.06	0.07	0.05	0.06	0.07	0.08	0.10
HIP96014	-0.35	-0.35	-0.35	-0.35	-0.35	-0.35	-0.35	-0.35	-0.35	-0.35	-0.35	-0.35
KIC3955590	0.05	0.05	0.05	0.05	0.05	0.05	0.05	0.05	0.05	0.05	0.05	0.05
KIC5113061	-0.12	-0.13	-0.13	-0.13	-0.13	-0.13	-0.13	-0.13	-0.13	-0.13	-0.13	-0.13
KIC5859492	0.13	0.13	0.13	0.13	0.12	0.13	0.13	0.13	0.13	0.13	0.13	0.13
KIC6465075	-0.26	-0.26	-0.26	-0.70	-0.27	-0.26	-0.26	-0.27	-0.26	-0.25	-0.25	-0.25
KIC6547007	-0.70	-0.70	-0.70	-0.08	-0.70	-0.75	-0.70	-0.69	-0.70	-0.69	-0.69	-0.74
KIC11444313	-0.08	-0.07	-0.07	-0.26	-0.08	-0.07	-0.07	-0.07	-0.07	-0.07	-0.07	-0.07
HD102328_K3III	0.28	0.28	0.28	0.28	0.28	0.28	0.28	0.28	0.28	0.28	0.28	0.28
HD142091_K0III-IV	0.10	0.10	0.10	0.10	0.11	0.10	0.10	0.11	0.11	0.10	0.11	0.11

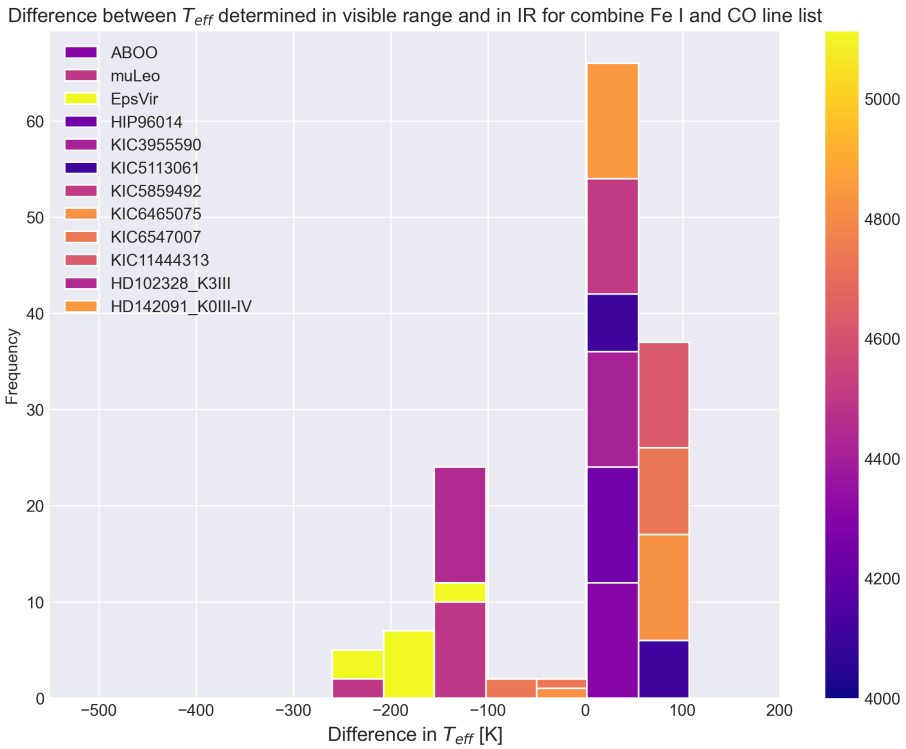

Figure D.1: Difference in $T_{\rm eff}$ between determined value and benchmark for combined Fe I and CO line list